NeuroImage 221 (2020) 117148

Contents lists available at ScienceDirect

NeuroImage

journal homepage: www.elsevier.com/locate/neuroimage

From shape to meaning: Evidence for multiple fast feedforward hierarchies of concept processing in the human brain

Srikanth R. Damera, Jacob G. Martin, Clara Scholl, Judy S. Kim, Laurie Glezer, Patrick S. Malone, Maximilian Riesenhuber *

Department of Neuroscience, Georgetown University Medical Center, Washington, DC, USA

A B S T R A C T

A number of fMRI studies have provided support for the existence of multiple concept representations in areas of the brain such as the anterior temporal lobe (ATL) and inferior parietal lobule (IPL). However, the interaction among different conceptual representations remains unclear. To better understand the dynamics of how the brain extracts meaning from sensory stimuli, we conducted a human high-density electroencephalography (EEG) study in which we first trained participants to associate pseudowords with various animal and tool concepts. After training, multivariate pattern classification of EEG signals in sensor and source space revealed the representation of both animal and tool concepts in the left ATL and tool concepts within the left IPL within 250 ms. Finally, we used Granger Causality analyses to show that orthography-selective sensors directly modulated activity in the parietal-tool selective cluster. Together, our results provide evidence for distinct but parallel "perceptual-to-conceptual" feedforward hierarchies in the brain.

1. Introduction

Humans can rapidly and efficiently assign meaning to visual objects. For visual stimuli, this process is traditionally thought to be mediated by the visual ventral stream, along which information is processed by a simple-to-complex hierarchy, up to neurons in ventral temporal cortex that are selective for complex objects such as faces, objects and words (Kravitz et al., 2013). According to computational models (Ashby and Spiering, 2004; Freedman et al., 2003; Nosofsky, 1986; Riesenhuber and Poggio, 2000; Thomas et al., 2006) as well as human functional magnetic resonance imaging (fMRI) and electroencephalography (EEG) studies (Jiang et al., 2007; Scholl et al., 2013), these object-selective neurons in high-level visual cortex can then provide input to task modules located in downstream cortical areas, such as prefrontal cortex (PFC) and the anterior temporal lobe (ATL), to mediate the identification, discrimination, or categorization of stimuli. It is at this level where these theories of object categorization in the brain connect with influential theories of semantic cognition that have proposed that the ATL may act as a "semantic hub" (Ralph et al., 2016), based on neuropsychological findings (Hodges et al., 2000; Jefferies, 2013; Mion et al., 2010) and studies that have used fMRI (Coutanche and Thompson-Schill, 2015; Malone et al., 2016; Vandenberghe et al., 1996) or intracranial EEG (iEEG) (Chan et al., 2011) to decode category representations in the anteroventral temporal lobe.

Yet, the processing of some object classes has been shown to involve additional pathways. A prominent example is the object class of tools, which, in addition to the ventral stream, engages the dorsal, "vision for action" (Goodale, 2011; Goodale and Milner, 1992; Kravitz et al., 2011) pathway, with areas in parietal cortex being selectively activated by tool stimuli, and lesions in parietal cortex affecting tool praxis (Buxbaum et al., 2014; Vingerhoets et al., 2009). A key, but unresolved, question in models of semantic processing is how the brain accesses these different types of concept knowledge. In particular, are there separate pathways that link sensory representations to distinct domain-specific concept representations, compatible with distributed models of semantic processing (Chen and Rogers, 2015), or does knowledge from one domain access that from another indirectly through representations in a domain-general hub (Almeida et al., 2013; Hodges et al., 2000)?

Resolving the question of how different types of concept knowledge are processed and interact requires the ability to not only delineate the underlying network of brain areas, but also, and crucially, the information flow between them. Recent fMRI research has uncovered a complex network of brain areas underlying semantic processing (Chen et al., 2017; Pulvermüller, 2013). Yet, due to its limited temporal resolution, fMRI is unable to directly probe the information flow within these networks, considering that numerous prior studies have shown that the brain is able to extract meaning from sensory stimuli within about 200 ms (Chan et al., 2011; Scholl et al., 2013; Thorpe et al., 1996), and, equally

* Corresponding author. Department of Neuroscience, Georgetown University Medical Center Research, Building Room WP-12, 3970 Reservoir Rd. NW Washington, DC, 20007, USA.

E-mail address: mr287@georgetown.edu (M. Riesenhuber).

https://doi.org/10.1016/j.neuroimage.2020.117148

Received 30 March 2020; Received in revised form 10 June 2020; Accepted 6 July 2020

Available online 11 July 2020

important, that neural processing dynamics do not just include a "feed-forward" flow of information, but also, starting within 150 ms and continuing for several hundred milliseconds, several re-entrant waves of activation, e.g., associated with stimulus awareness (Cul et al., 2007; Fahrenfort and Lamme, 2012), whereas typical fMRI scan paradigms have temporal resolutions that are ten times slower. In contrast, EEG with its millisecond resolution is better matched to the speed of visual processing in the brain. We used a combination of multivariate pattern analysis (MVPA) and EEG to address these challenges and gain a better understanding of the dynamics of the neural networks underlying concept processing. We trained participants to associate a vocabulary of pseudowords (PWs) with various animal and tool categories (Fig. 1A). Next, we collected high-density EEG data while subjects performed a delayed-match-to-sample task. We applied searchlight MVPA in sensor as well as source space to temporally and spatially localize concept information in the brain. In addition, Granger Causality analyses were used to elucidate the dynamics of signal flow within the semantic network.

2. Materials and Methods

2.1. Participants

A total of 11 right-handed healthy adults who were native English speakers were enrolled in the experiment (ages 20–29, 5 females). Georgetown University's Institutional Review Board approved all experimental procedures, and written informed consent was obtained from all subjects before the experiment.

2.2. Behavioral training

PWs (all four letters in length) matched for bigram and trigram frequency, and orthographic neighborhood were generated using MCWord (Medler and Binder, 2005). Subjects were trained to learn a vocabulary of 60 PWs, with each PW assigned to one of six categories: monkey, donkey, elephant, hammer, wrench, and screwdriver (i.e., 10 PWs were defined as "monkey," 10PW as "donkey," etc.). To learn the PW definitions, each subject performed 0.5–1 h of training per session for a total of 8 sessions in which a PW was presented on a screen followed by 6 pictures: one picture for each of the animal and tool categories (randomly selected from a large database of images for each category to prevent subjects from associating particular words with particular images). Subjects indicated their category choice using a numeric keypad. When subjects answered incorrectly, an auditory beep and the correct answer were presented. No feedback was given for correct answers. A single training session consisted of 5 blocks, and a unique set of 2 PWs (within the 10 per category) was used for each block to facilitate learning.

2.3. EEG paradigm

Following training, we probed the neural bases of the learned concept memberships using an EEG paradigm. Each trial of the EEG experiment consisted of a fixation cross for 500 ms, a blank screen for 200 ms with jitter, followed by the first PW for 300 ms, blank screen for 400 m, and second PW for 300 ms. Following the second PW, subjects were instructed to indicate with a button click if both words referred to the same or different superordinate categories (Fig. 1B). Trials were broken into four different conditions depending on the relationship between the first and second PWs: same word/same basic-level category (SWSC), different word/same basic-level category (DWSC, e.g., first: monkey PW, second: a different monkey PW), different word/different basic-level category (DWDC, e.g., first: monkey PW, second: a donkey PW), and different word/different superordinate category (DWDSC, e.g., first: animal PW, second: a tool PW). Each subject participated in a single session with two runs each. Each run had three blocks, each of which were 136 trials long, for a total of 408 trials in a run. Counts for the four trial types were matched in each session and different conditions were presented in a random manner. Trials with incorrect responses were removed from the analyses. In this study, only data from the first PW presentation were analyzed for the decoding analyses.

2.4. EEG data acquisition and preprocessing

Scalp voltages were measured using an Electrical Geodesics (EGI, Eugene, OR) 128-channel Hydrocel Geodesic Sensor Net and Net Amps 300 amplifier. Incoming data were digitally low-pass filtered at 200 Hz and sampled at 500 Hz using common mode rejection with vertex reference. Impedances were set below 40 kΩ before recording began and maintained below this threshold throughout the recording session with an impedance check during each break between blocks.

Pre-Processing: Data processing and statistical analyses were performed using EEGLAB (Delorme and Makeig, 2004). Data were first high-pass filtered at 0.2 Hz and then low-pass filtered at 30 Hz. A minimum-phase causal filter ensured that information did not get smeared backwards and was used for decoding analyses to accurately determine the onset latency of classification (Widmann and Schröger, 2012). Bad channel identification was automated using the clean_rawdata EEGLab plugin that cleaned continuous data using artifact subspace reconstruction. Bad channels identified with this method were then reconstructed using spherical interpolation. Continuous data were epoched on the interval of [-200 300] ms relative to the onset of the first word. The mean of the baseline period was then subtracted from the signal. Bad trials were marked if the voltage exceeded ±50 μV on any EEG channel. Finally, the data were re-referenced to average reference since this has been shown to improve the quality of the source reconstruction (Dien, 1998).

2.5. EEG source estimation

Source reconstruction was conducted using common forward and inverse models implemented in Brainstorm (Tadel et al., 2011). In Brainstorm (version 11-13- 2019), the EEG forward problem was solved in the ICBM152 template anatomy. Realistically-shaped volume meshes of the brain, skull and scalp were extracted from the provided template MR image using the default number of 1922 vertices per layer for a total of 15765 sources. The forward model (lead field) from these source locations to the 128 channels was calculated using the symmetric boundary Element method as implemented in the Open-MEEG package. Inverse estimation of sources was carried out using the LCMV Beamformer. The noise covariance matrix for this method was built using the 200 ms of baseline data, and the data covariance matrix was constructed using the 300 ms of word presentation.

2.6. MVPA decoding

MVPA analyses were performed using The Decoding Toolbox (Hebart et al., 2014) and custom MATLAB code (R2017b, The Mathworks, MA). All classifications implemented a linear support vector machine (SVM) classifier with a fixed cost parameter ($c = 1$). For each subject, all trials of a particular PW were averaged over the entire session so that a single pseudo-trial was created for each PW. This procedure has been shown to increase the signal-to-noise-ratio (Grootswagers et al., 2016). 100-fold Monte Carlo cross-validation was performed with an approximate 50/50 training to testing split. Training and testing sets were carefully partitioned so that no PW was included in both the training and testing set within a fold. Accuracies were averaged across folds to compute an unbiased measure of classifier performance.

Sensor Space Spatiotemporal Searchlight Decoding: Time-resolved spatial decoding analyses were then performed in sensor space. For these decoding analyses, a 3 cm searchlight was constructed around each sensor (searchlight size ranged from 1 to 7 sensors, but similar results were obtained with a 4 cm searchlight which had a range of 3–8 sensors in a searchlight). Temporal data for each sensor in a given

searchlight were averaged in order to create an N-channel-by-1 feature vector per searchlight. This was done in 20 ms windows and advanced 2 ms over the duration of the word (Fig. 1C).

Source Space Spatial Decoding: To spatially localize sensor level classification, voltage data were projected to source space (see above) and a searchlight MVPA was performed using a 10 mm searchlight. The value at a given source was taken as the average over a time window of interest defined by sensor level decoding results (Fig. 1D).

2.7. MVPA analysis 1 (superordinate classification)

For each subject, an animal versus tool classification was first performed in sensor space to identify the onset latency and time window of superordinate decoding. Within each cross-validation fold, the classifier was trained on 40 PWs (20 animal and 20 tool PW) and tested on the remaining 20 PWs. Once a significant time-window of decoding was identified at the sensor level, this time window was then submitted to the classification procedure in source space in order to estimate a neuroanatomical source of the classification.

2.8. MVPA analysis 2 (basic-level classification)

Next, a within-category classification was performed in sensor space to identify the onset latency and time window of basic-level decoding. There was a total of 6 (3 within-animal and 3 within-tool) unique classifications. One subject was not shown any elephant or wrench PWs and was excluded from the basic-level classification analyses. Within each cross-validation fold, the classifier was trained on 10 PWs (e.g., 5 hammer and 5 wrench PWs) and tested on the remaining 10 PWs. The resulting spatiotemporal classification maps for all within-animal comparisons were averaged to produce a single accuracy map for basic-level animal concepts. This was repeated for all within-tool comparisons as well. Once a significant time-window of decoding was identified at the sensor level this was then submitted to the classification procedure in source space in order to estimate a neuroanatomical source of the classification.

2.9. Statistical analysis of classification results

Each MVPA analysis produced an accuracy value at each sensor or source. At the group-level, multiple comparisons across sensors and time-points or sources was done using cluster-mass correction (Maris and Oostenveld, 2007). For this method, an empirical null distribution was constructed for each subject at every sensor and time-point by permuting labels across the entire data set, setting up cross-validation folds, and then performing the classification procedure as before. This procedure was repeated 1000 times, and then the observed and null distributions were averaged across subjects at every sensor and time point. The p-value associated with the accuracy observed at a single electrode time-point combination was calculated as the proportion of values in the null distribution greater than the observed value. Next, an initial cluster level threshold, α, was used to generate either spatiotemporal or spatial clusters corresponding to sensor space and source space analyses, respectively. α was set to .002, for both sensor and source space analyses. Previous fMRI studies have noted that a liberal α (i.e., >0.001) increases the rate of false positives (cf. Fig. 1 in Eklund et al., 2016). However, this is specific to parametric approaches using random field theory and not non-parametric permutation-based approaches (Eklund et al., 2016). It

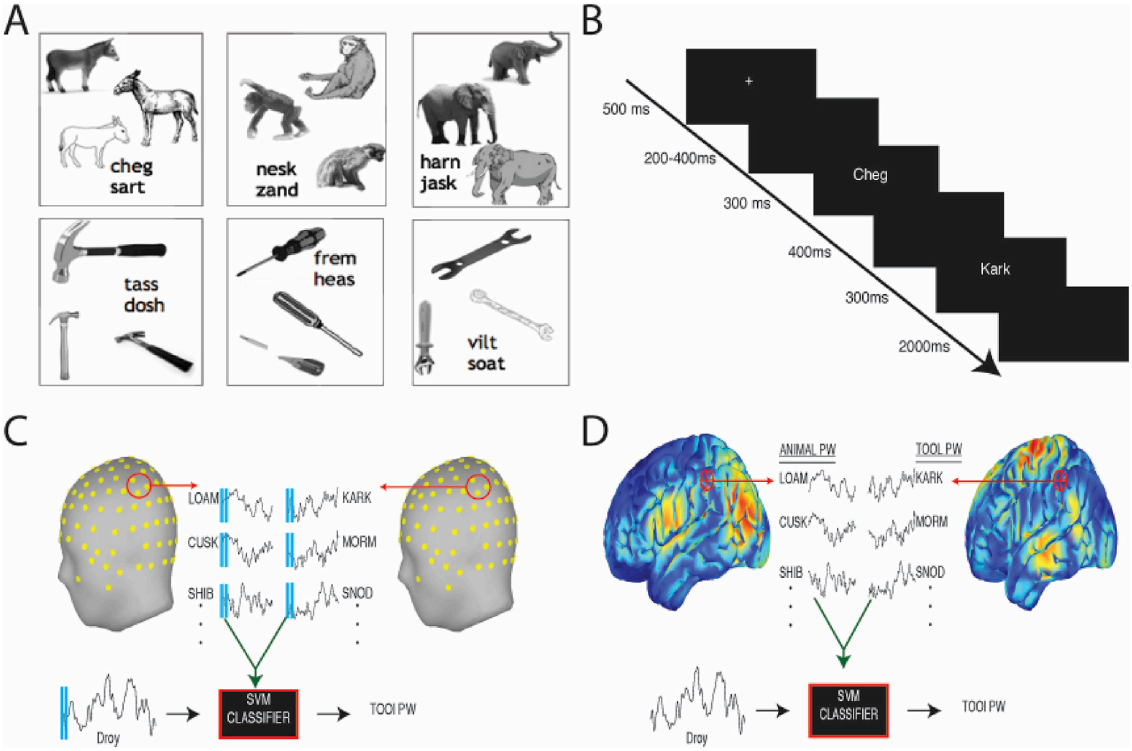

Fig. 1. Task and analysis paradigms. (A) Subjects were trained on a set of 60 pseudowords (PW) belonging to one of three animal or tool categories (two PWs are shown as examples with each category), as in Malone et al. (2016). (B) After training, subjects participated in an EEG experiment, in which they performed a delayed-match-to-superordinate category task in which two PWs were sequentially presented on each trial and subjects had to indicate after the presentation of the second word if both words belonged to the same or different superordinate categories (i.e., animals or tools). (C) At each sensor and for different time bins (the blue shaded region illustrates one example time bin), a set of time-lagged support vector machine (SVM) classifiers was constructed on half the trained pseudowords (PWs) from animal and tool categories and then tested on the other half, resulting in dynamic classification accuracy maps for each subject in sensor space. (D) In separate analyses, EEG sensor data were projected into source space (see Materials and Methods), followed by averaging over a time period of interest. Searchlight MVPA was then performed, resulting in a spatial accuracy map per subject.

has been shown that permutation-based methods control the false positive rate at the desired level independent of the α chosen (Maris and Oostenveld, 2007; Sassenhagen and Draschkow, 2019; Woo et al., 2014). The mass of clusters was computed by summing the accuracies of all the sensors or sources in the cluster. The mass of each cluster in the actual data was compared to an empirical distribution of maximal clusters of the permuted data and was marked as significant if it was greater than 95% of the values.

2.10. Identification of clusters selective for orthography

Orthographically-selective space-time clusters were identified by contrasting responses to the second words in each trial in the SWSC and DWSC conditions, and significance was assessed using cluster-based permutation testing. Due to strong *a priori* hypotheses about the latency of the N170 response to words (Brem et al., 2010; Dehaene et al., 2015; Maurer et al., 2005) this analysis was constrained to left lateralized sensors between 100 and 200 ms after the onset of the second word. Using fMRI and EEG it has been shown that neuronal populations that are selective for a feature of interest (e.g., orthography) have a reduced (adapted) response for rapidly presented pairs of stimuli that are consistent versus inconsistent for that feature (Glezer et al., 2009; Jiang et al., 2007; Scholl et al., 2013). In the current study, we hypothesized that sensors recording from populations of neurons sensitive to orthography would exhibit an adapted N170 response to sequential presentation of the same PW versus presentation of two different PWs. Crucially, to control for differences due to semantics, we used SWSC and DWSC trials in which both the first and the second word referred to the same basic-level concept. As for the classification results, spatiotemporal clusters were identified by setting the cluster-defining α to 0.002 and then their significance was controlled at the two-tailed $p < .05$ level.

2.11. Granger Causality

Granger Causality (Granger, 1969) (GC) has been used to investigate causal relationships between prefrontal and early visual neural recording sites in monkey and human electrophysiology recordings (Cui et al., 2008; Gregoriou et al., 2009; Seth et al., 2015). In this work, we computed Granger Causality within each subject at the single trial level between all pairs of channels in the left anterior temporal superordinate-classification, parietal basic-level tool, and left posterior orthographic sensors (see Fig. 5A). We used the BSMART toolbox (Cui et al., 2008) with a model order of 15 and a sliding temporal window of 60 ms. We only used artifact-free trials for which correct responses were given. Before computing the Granger Causality, we performed the standard preprocessing step of subtracting the temporal mean of each trial (in each channel) from all data points in that trial. Next, we calculated the Granger causalities for each time point and subject separately for each channel pair. Finally, we averaged the frequency-specific Granger Causality values for all channel pairs into the theta (4–7 Hz), alpha (8–12 Hz), and beta (13–30 Hz) frequency bands for each condition and subject to obtain a time-based version of Granger Causality within that subject, and frequency band.

2.12. Statistical analysis of Granger Causality results

A mixed effects modelling approach was taken to test the significance of Granger Causality effects. Models were built to test when the GC of each of the proposed pathways (e.g., orthography to basic-level tool selective sensors) deviated from baseline. The model included a fixed-effect of frequency band, and a random-effect of subjects. Since orthographic processing indexed by the N170 ERP begins at ~150 ms, this model was constructed at each time point between 150 and 300 ms, and two-tailed p-values for the fixed-effects of interest were FDR-corrected at the .05 level to control for multiple comparisons across time and frequency bands.

3. Results

3.1. Behavior

Each subject ($n = 11$) performed 8 training sessions over an average of 13.8 days (SD ±3.2). Subjects performed only a single training session per day. Both accuracy and RT for identification of PW category improved across training sessions (Fig. 2A). On average, subjects reached an accuracy of 98.7% by their eighth training session. During the delayed-match-to-basic-level category task, subjects reached 93.7% accuracy on average (Fig. 2B). A two-way ANOVA with the factors condition (same word/same basic category, SWSC; different word/same basic category, DWSC; different word/different basic category, DWDC; different word/different superordinate category, DWDSC) and superordinate category (animals and tools) of the first word in each trial was conducted in order to test for any effect of condition or superordinate category on task performance. This revealed a significant main effect of condition on accuracy ($F_{(3,79)} = 6.88$, two-tailed $p = 0.004$). Importantly, there was no significant main effect of superordinate category on task accuracy ($F_{(1,79)} = 1.78$, two-tailed $p = 0.18$). In order to investigate the source of the significant effect of condition, post-hoc t-tests comparing accuracy between all pairs of conditions showed that there was a significant difference in accuracy for SWSC vs. DWSC (two-tailed $p = 0.002$) contrast as well as the DWDSC vs. DWSC (two-tailed $p = 0.008$) contrast. There was no significant interaction between superordinate category and condition on accuracy ($F_{(3,79)} = 1.03$, two-tailed $p = 0.39$).

3.2. EEG single-trial analysis reveals fast superordinate concept selectivity over temporal sensors, localized to the ATL

We conducted a series of single-trial classification analyses of the EEG signal in response to the first word in each trial to analyze how the brain maps sensory stimuli to concepts. We first explored the onset of superordinate-level (animals vs. tools) information at the sensor level within the 100–300 ms interval. This revealed one spatiotemporal cluster with significantly above-chance classification performance (Fig. 3A and B). The left-anterior temporal cluster was significantly above chance from 204 to 268 ms post-word presentation with peak accuracy at 236 ms (Fig. 3B; cluster-defining $\alpha = 0.002$, one-tailed $p = .0240$, see Material and Methods). We then projected sensor data to source space using an LCMV (Linearly Constrained Minimum Variance) beamformer (Grech et al., 2008) to localize the cortical source(s) of this classification. Furthermore, to better characterize the timing of concept processing in our broad temporal cluster (204–268 ms) (Sassenhagen and Draschkow, 2019), we separately averaged source maps in the early (204–236 ms) and late (236–268 ms) halves of the cluster (see Materials and Methods). We hypothesized that concept information in the ATL should localize to the early rather than late time window, given our overarching hypothesis that activation of concept information in ATL would be the next step in the ventral stream processing hierarchy following the orthographic representation (which has been associated with the N170 in the literature (Brem et al., 2010; Dehaene et al., 2015; Maurer et al., 2005), with a temporal extent from about 170 to 200 ms), taking into account estimates in the literature of each cortical processing stage taking on the order of 30 ms (Thorpe and Fabre-Thorpe, 2001). Searchlight source space analysis indeed localized superordinate category information in the early time window to the LATL (Fig. 3C; cluster-defining $\alpha = 0.002$, one-tailed $p = .025$).

3.3. EEG single-trial analysis reveals fast basic-level decoding of tools in left parietal sensors

We next examined the latency and location of basic-level (within-tool and within-animal) category decoding. We identified sensors that distinguished among the different tools: Sensor-level searchlight analysis between 100 and 300 ms after stimulus onset revealed a

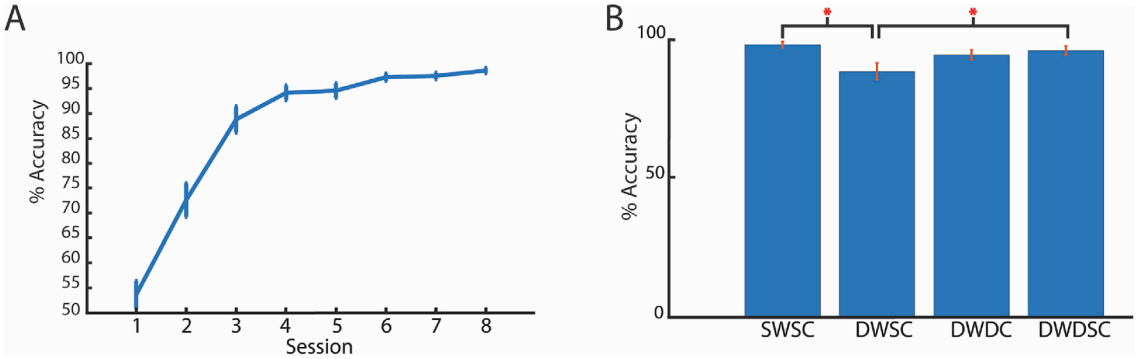

Fig. 2. Pseudoword training performance and delayed-match-to-superordinate category task accuracy. (A) Mean accuracies for identification of pseudoword category across training sessions during a 6 alternative-forced choice task (n = 10). (B) Accuracy in the delayed-match-to-superordinate category task during which EEG data was collected for each condition: SWSC, first and second word were identical; DWSC, second word was different word, same basic-level category as the first word; DWDC, second word was different word, belonging to different basic-level category than the first word; DWDSC, second word was different word, different superordinate category than the first word. Brackets indicate significant differences across conditions: *p < 0.01; n = 11. Errors bars indicate SEM across subjects.

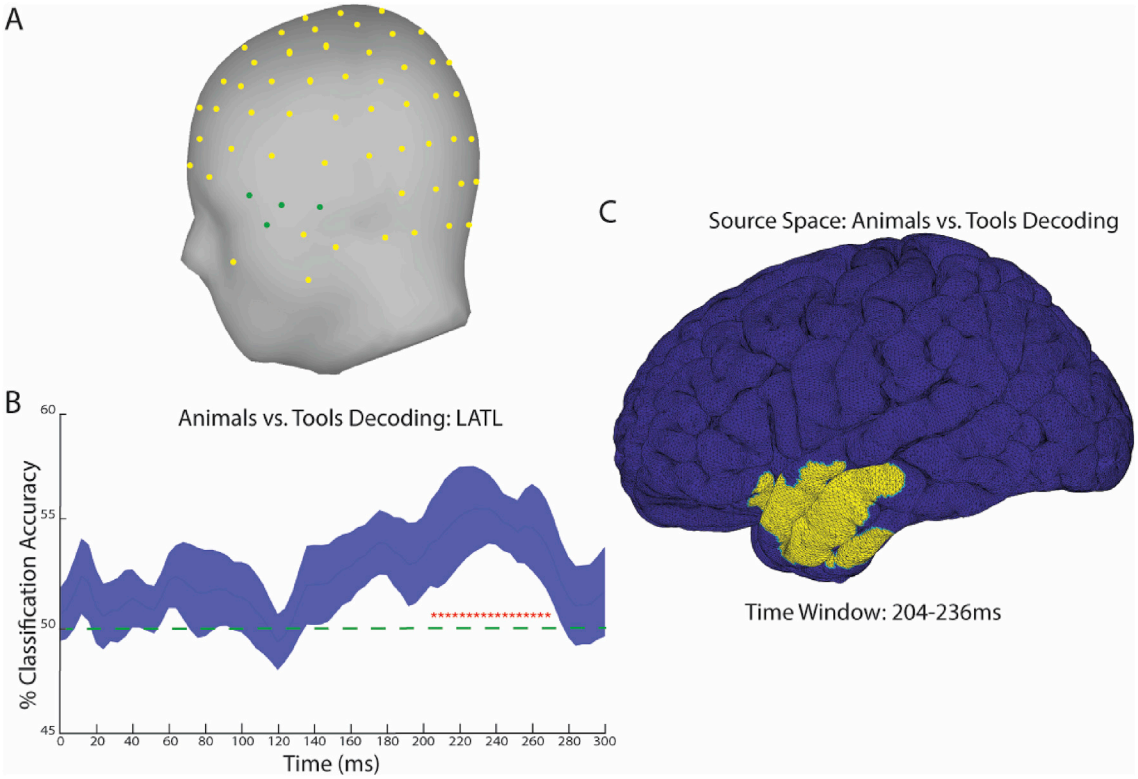

Fig. 3. Timing and location of superordinate classification of PW concept membership in sensor and source spaces and comparison to previous, fMRI results. (A) The spatial topography of the sensors that showed significant decoding of animal and tool PWs. Green sensors are referred to as "left anterior" cluster. (B) Time course of classification accuracy averaged across all sensors in the left anterior cluster. Red asterisks show time-window of significant classification, which extends from 204 to 268 ms post-word presentation (n = 11; α < 0.002; one-tailed p = .024). Shading shows SEM across subjects. (C) Source estimation of Animals vs. Tools classification. The locus of above-chance classification was investigated in an early (204–236 ms) and late (236–268 ms) time window. Activity in the early, but not the late time-window was estimated in source space to the LATL (n = 11; α < 0.002; one-tailed p = .025).

cluster of left posterior sensors that show significantly above-chance classification from 208 to 228 ms post-stimulus onset with peak accuracy at 220 ms (Fig. 4A and B; cluster-defining α = 0.002, one-tailed p = .031). Searchlight source space analysis localized the classification from this time period to the left inferior parietal lobe (Fig. 4C; cluster-defining α = 0.002, one-tailed p = .025. We also conducted basic-level animal classification, but no significant spatiotemporal clusters were found.

3.4. Granger Causality analysis supports feedforward "simple-to-concept" hierarchy

The latency of concept information in the preceding analyses provides evidence for fast, feedforward concept processing areas in the brain. The regions identified are compatible with the ventral and dorsal concept processing streams discussed in the Introduction. We next used Granger Causality analyses (Granger, 1969) to test if a common perceptual representation could be used to access these different

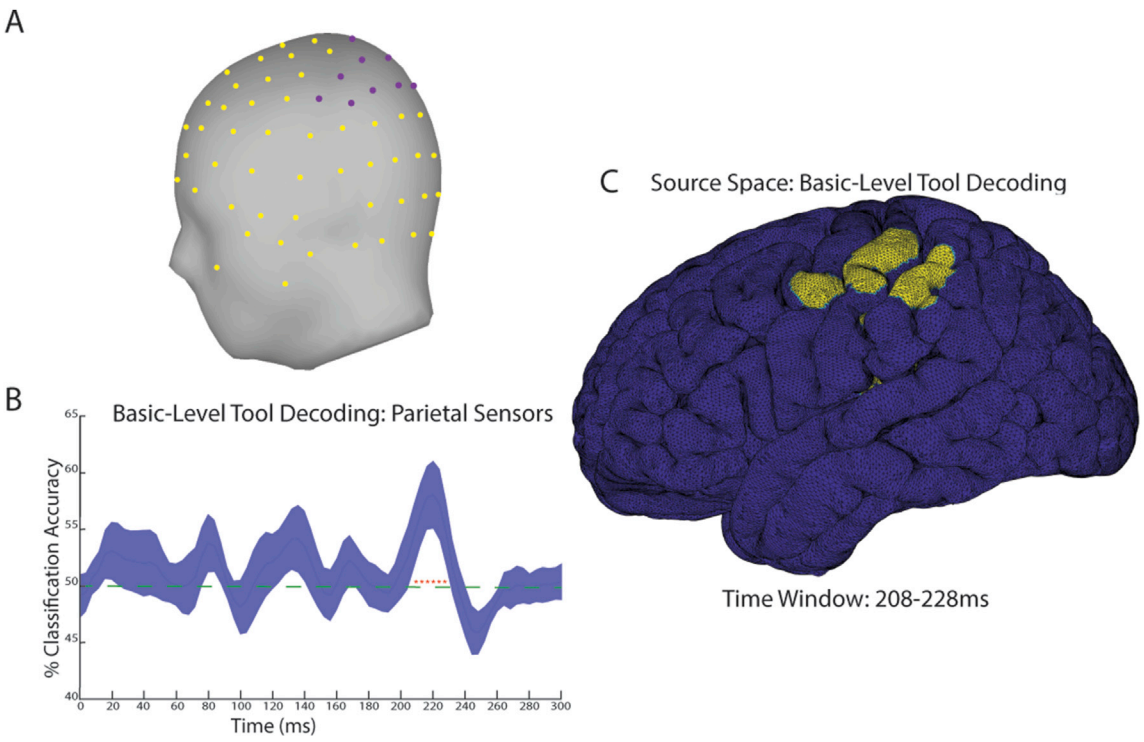

Fig. 4. Timing and location of tool classification of PW concept membership in sensor and source space. (A) The spatial topography of the sensors (shown in purple) that show significant decoding of tool PWs. (B) Time course of classification accuracy averaged across all sensors in the cluster. Red asterisks show time-window of significant classification, which extends from 208 to 228 ms post-word presentation ($n = 10$; $\alpha < 0.002$; one-tailed $p = .031$), shading shows SEM across subjects. (C) Source estimation of within-tools classification shown in panels A and B. The locus of above-chance classification during the time window of classification was estimated in source space to the left parietal lobe ($n = 10$; $\alpha < 0.002$; one-tailed $p = .025$).

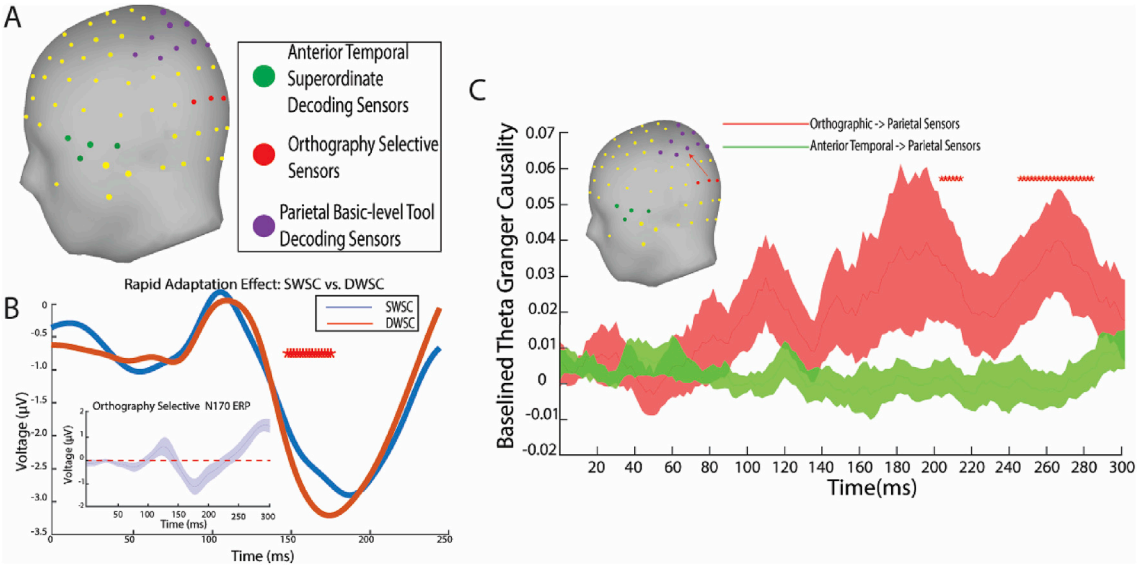

Fig. 5. Neural dynamics in the concept processing network. (A) The three seeds are marked orthographic (red), superordinate (green, see Fig. 3), and basic-level tool-selective (purple, see Fig. 4) sensor groups. (B) Average ERP of all sensors that show an orthographic response (shown in red in (A)) shows significant adaptation of the N170 response between 148 and 178 ms. Red asterisks mark the time window of the significant cluster ($n = 11$; $\alpha<0.002$; one-tailed $p = .034$). Average ERP of all sensors that show an orthographic response (shown in (A)) shows an N170 response during the first word (inset). (C) Baseline-normalized Granger Causality (GC) from orthographic (red) and anterior temporal (green) to parietal basic-level tool selective sensors in the theta frequency band. Red asterisks mark time points exhibiting significant increase in GC relative to baseline between orthographic and basic-level parietal tool selective sensors from 204 to 214 ms and from 246 to 284 ms ($n = 11$; two-tailed $p < .05$, FDR-corrected).

conceptual representations – a key prediction of two-stage models of category learning. Specifically, we investigated whether activity at orthographically-selective sensors directly modulated activity in dorsal tool-selective sensors. To do so, we first identified a high-level perceptual (orthography) selective cluster (Fig. 5A; see methods), putatively identifying the "visual word form area", VWFA (Brem et al.,

2010; Dehaene-Lambertz et al., 2018; Maurer et al., 2005) – the highest orthographically selective stage in the ventral visual pathway. This cluster showed a significant adaptation effect between 148 and 178 ms with a peak difference at 162 ms (Fig. 5B; cluster-defining $\alpha = 0.002$, two-tailed $p = .034$). This orthographic N170 cluster overlapped in both space and time with those reported in previous EEG studies (Maurer et al., 2005; Scholl et al., 2013). The ERP for these sensors showed an N170 response during the first word with the negative deflection starting at 150 ms post-stimulus onset (Fig. 5B inset). The sensors in this cluster were used as our orthographic seed.

We next calculated the change in Granger Causality (GC) relative to a 200 ms pre-stimulus baseline among the orthographically-selective sensors and the sensors representing concept information in the ventral and dorsal pathways that were identified in the previous sections. To examine if orthographic information directly accessed parietal tool-selective representations, we tested the change in GC between orthography and parietal-tool selective sensors from baseline in the theta (4–7 Hz) frequency band, which has been implicated in feedforward information flow (Bastos et al., 2014), as well as the alpha (8–12 Hz) and beta (13–30 Hz) frequency bands. After FDR correction across the three frequency bands and time points (see Materials and Methods), we found evidence that theta-frequency (but not alpha or beta) activity in orthography-selective sensors significantly modulated activity in parietal tool-selective sensors from 204 to 214 ms and 244–284 ms post-stimulus onset – just prior to the onset of basic-level tool representations (Fig. 5C; two-tailed $p < .05$ FDR corrected).

4. Discussion

The current study applied multivariate searchlight decoding of EEG data from a word learning paradigm to cleanly dissociate perceptual and conceptual information in the neural signals at high temporal resolution. This approach allowed us to address two key unanswered questions: when do different conceptual representations come online, and how are they accessed by sensory input? We provide evidence for superordinate category selectivity in left anterior sensors within 250 ms after word presentation. Using source estimation techniques, this selectivity was localized to the left anterior temporal lobe (LATL). Basic-level tool category membership was also decoded in a set of left parietal sensors between 208 and 228 ms after word presentation. The cortical generator of this signal was source estimated to the left parietal lobe. Importantly, these source-estimated ROI matched well with our previous fMRI study that used the same training paradigm (Malone et al., 2016). Finally, we used Granger Causality to investigate how high-level perceptual information feeds into different conceptual representations in the brain. This analysis revealed that orthography-selective sensors Granger-caused activity in tool-selective sensors in the dorsal stream between 204 and 214 ms.

Our results show that concept-selective circuits receive rapid, feedforward input from perceptual (orthographic) representations. This finding is consistent with the aforementioned two-stage models of category learning (Ashby and Spiering, 2004; Riesenhuber and Poggio, 2002, 2000), which predict that learned perceptual representations can be flexibly recruited by distinct higher-order circuits in order to accomplish different tasks. These two-stage models make clear predictions regarding the latency of concept-selective circuits, predicting that, due to their putative location in the cortical hierarchy following object-selective representations which have been associated with the N170 EEG signal component (Gauthier et al., 2003; Pegado et al., 2014; Rossion et al., 2002; Tanaka and Curran, 2001), they should be activated around 200 ms (Thorpe and Fabre-Thorpe, 2001). Yet, the temporal onset of concept-level processing is still debated (Carreiras et al., 2014), with many studies claiming that concept representations (frequently localized to the ATL (Coutanche and Thompson-Schill, 2015; Jackson et al., 2015; Lau et al., 2008; Ralph et al., 2016) are activated around 400 ms post-stimulus onset (Kutas and Federmeier, 2011; Jackson et al., 2015). Our results add to a growing body of literature (Bankson et al., 2018; Chan et al., 2011; Clarke et al., 2011) showing that concept information comes online prior to 250 ms post-stimulus onset, indicating that concept processing can be understood as a straightforward extension of Hubel and Wiesel's "simple-to-complex" feedforward model of visual processing from visual to concept processing. The qualitatively sustained rise in classification accuracy above chance starting at ~160 ms post-stimulus onset (Fig. 3B) suggests that the true onset of concept information may be even earlier than identified in our study. Our results are in line with a recent study that used a combination of behavioral modeling, deep neural networks, and MEG to estimate the lower-bound of semantic processing in the visual ventral stream at ~150 ms and a peak processing at ~230 ms (Bankson et al., 2018).

Of note, we find the rapid onset of concept representations not only in left anterior temporal sensors, but also in left parietal sensors. Previous work (Garcea et al., 2018; Ishibashi et al., 2011; Pobric et al., 2010) showed evidence that left parietal tool representations encode tool manipulation knowledge, and LATL representations store tool function knowledge. The interplay between these representations, and to what degree access to one relies on access to the other is unclear. In certain theories of semantic cognition, the ATL serves as a "semantic hub" that integrates over different attributes (shape, manipulability, sound, etc.) of a concept and helps coordinate interactions between them (Patterson et al., 2007; Ralph et al., 2016). Thus, some have suggested that degeneration of the hub in semantic dementia precludes access to manipulation knowledge in the visual dorsal stream via shape representations in the visual ventral stream (Almeida et al., 2013; Hodges et al., 2000). However, other lesion and TMS studies show that tool manipulation knowledge can be accessed even when tool function knowledge is impaired and vice versa (Buxbaum et al., 2000; Buxbaum and Saffran, 2002; Garcea and Mahon, 2012; Ishibashi et al., 2011). Our study supports the latter view by showing a direct feedforward functional pathway between orthographic representations, likely in posterior fusiform cortex, and left parietal tool representations that is independent of the LATL. This is supported by DTI studies (Binder and Desai, 2011; Wakana et al., 2004) that show direct anatomical connections between the VWFA and LIPL, which could underlie the direct Granger-causal connectivity seen in our data. An important limitation of the current work is that we were unable to identify a parallel pathway between orthography-selective sensors and anterior concept-selective sensors in our data. However, the existence of feedforward anatomical connections from posterior fusiform cortex to anterior temporal areas has been well established (Bouhali et al., 2014; Kravitz et al., 2013; Papinutto et al., 2016). Furthermore, in the context of concept processing, Clarke et al. (2011) in a MEG study identified a cluster of significant phase-locking between posterior shape selective and anterior concept selective sensors in the gamma frequency between 120 and 220 ms. Thus, the literature provides strong existing evidence for a ventral pathway from orthography to concepts, and the novelty of our study lies in showing the existence of a parallel ventral-to-dorsal stream pathway from orthography-selective ventral stream areas to parietal cortex.

A notable aspect of our results is that the direct pathway between orthography and parietal tool concepts exists after training despite the fact that tool PW orthography, unlike tool images, does not contain any visual features that could be leveraged to automatically access dorsal stream manipulation information. Furthermore, our training paradigm did not explicitly train participants on the association between orthography and manipulation. This raises the intriguing question of how this dorsal word-to-manipulation knowledge network is learned. Findings from a recent computational investigation (Chen and Rogers, 2015) suggest that feedback from other conceptual representations can help set up this shape-to-manipulation pathway. In that study, the authors implemented a connectionist model in which units encoding shape representations in the visual ventral stream were linked to concept units representing a semantic hub and to a separate set of concept units

representing manipulation knowledge. In this model, as validated by our results, information from shape units directly engaged the correct information in the manipulation units after training. In addition, they found that hub units exerted a feedback influence on shape units, which in turn influenced correct access to manipulation information. This feedback from the semantic hub units could suggest a mechanism by which the proper connections between mid-fusiform and parietal regions can be set up. Alternatively, given its extensive connections with parietal cortex, regions in prefrontal cortex (Friederici, 2009; Ruschel et al., 2014; de Schotten et al., 2011) (e.g., in the inferior frontal gyrus, known to be involved in semantic processing) could be involved in coordinating the learning of these multiple perceptual-to-conceptual hierarchies in the brain.

In summary, our results indicate that multiple perceptual-to-conceptual hierarchies, once learned, exist independently of each other in the brain, allowing fast, feedforward computation of function and manipulation knowledge, respectively. Further work needs to be done to understand how different types of representation interact with each other to set up these hierarchies in the brain.

Declaration of competing interest

The authors declare no competing financial interests.

CRediT authorship contribution statement

Srikanth R. Damera: Formal analysis, Investigation, Writing - original draft, Writing - review & editing. **Jacob G. Martin:** Formal analysis, Writing - review & editing. **Clara Scholl:** Conceptualization, Methodology, Investigation. **Judy S. Kim:** Conceptualization, Methodology, Investigation. **Laurie Glezer:** Conceptualization, Methodology, Investigation. **Patrick S. Malone:** Methodology. **Maximilian Riesenhuber:** Supervision, Conceptualization, Methodology, Writing - original draft, Writing - review & editing, Funding acquisition.

Acknowledgements

This work was supported by National Science Foundation Grant 1026934 to M.R., National Science Foundation Grant PIRE OISE-0730255, and NIH Intellectual and Development Disorders Research Center Grant 5P30HD040677.

References

Almeida, J., Fintzi, A.R., Mahon, B.Z., 2013. Tool manipulation knowledge is retrieved by way of the ventral visual object processing pathway. Cortex 49, 2334–2344. https://doi.org/10.1016/j.cortex.2013.05.004.

Ashby, G.F., Spiering, B.J., 2004. The neurobiology of category learning. Behav. Cognit. Neurosci. Rev. 3, 101–113. https://doi.org/10.1177/1534582304270782.

Bankson, B.B., Hebart, M.N., Groen, I.I.A., Baker, C.I., 2018. The temporal evolution of conceptual object representations revealed through models of behavior, semantics and deep neural networks. Neuroimage 178, 172–182. https://doi.org/10.1016/j.neuroimage.2018.05.037.

Bastos, A.M., Vezoli, J., Bosman, C.A., Schoffelen, J.-M., Oostenveld, R., Dowdall, J.R., Weerd, P.D., Kennedy, H., Fries, P., 2014. Visual areas exert feedforward and feedback influences through distinct frequency channels. Neuron 85, 390–401. https://doi.org/10.1016/j.neuron.2014.12.018.

Binder, J.R., Desai, R.H., 2011. The neurobiology of semantic memory. Trends Cognit. Sci. 15, 527–536. https://doi.org/10.1016/j.tics.2011.10.001.

Bouhali, F., de Schotten, M., Pinel, P., Poupon, C., Mangin, J.-F., Dehaene, S., Cohen, L., 2014. Anatomical connections of the visual word form area. J. Neurosci. 34, 15402–15414. https://doi.org/10.1523/JNEUROSCI.4918-13.2014.

Brem, S., Bach, S., Kucian, K., Kujala, J.V., Guttorm, T.K., Martin, E., Lyytinen, H., Brandeis, D., Richardson, U., 2010. Brain sensitivity to print emerges when children learn letter–speech sound correspondences. Proc. Natl. Acad. Sci. Unit. States Am. 107, 7939–7944. https://doi.org/10.1073/pnas.0904402107.

Buxbaum, L.J., Saffran, E., 2002. Knowledge of object manipulation and object function: dissociations in apraxic and nonapraxic subjects. Brain Lang. 82, 179–199. https://doi.org/10.1016/S0093-934X(02)00014-7.

Buxbaum, L.J., Shapiro, A.D., Coslett, B.H., 2014. Critical brain regions for tool-related and imitative actions: a componential analysis. Brain 137, 1971–1985. https://doi.org/10.1093/brain/awu111.

Buxbaum, L.J., Veramontil, T., Schwartz, M.F., 2000. Function and manipulation tool knowledge in apraxia: knowing 'what for' but not 'how. Neurocase 6, 83–97. https://doi.org/10.1080/13554790008402763.

Carreiras, M., Armstrong, B.C., Perea, M., Frost, R., 2014. The what, when, where, and how of visual word recognition. Trends Cognit. Sci. 18, 90–98. https://doi.org/10.1016/j.tics.2013.11.005.

Chan, A.M., Baker, J.M., Eskandar, E., Schomer, D., Ulbert, I., Marinkovic, K., Cash, S.S., Halgren, E., 2011. First-pass selectivity for semantic categories in human anteroventral temporal lobe. J. Neurosci. 31, 18119–18129. https://doi.org/10.1523/JNEUROSCI.3122-11.2011.

Chen, L., Ralph, M.A., Rogers, T.T., 2017. A unified model of human semantic knowledge and its disorders. Nat. Human Behav. 1 https://doi.org/10.1038/s41562-016-0039, 0039.

Chen, L., Rogers, T.T., 2015. A model of emergent category-specific activation in the posterior fusiform gyrus of sighted and congenitally blind populations. J. Cognit. Neurosci. 27, 1981–1999. https://doi.org/10.1162/jocn_a_00834.

Clarke, A., Taylor, K.I., Tyler, L.K., 2011. The evolution of meaning: spatio-temporal dynamics of visual object recognition. J. Cognit. Neurosci. 23, 1887–1899. https://doi.org/10.1162/jocn.2010.21544.

Coutanche, M.N., Thompson-Schill, S.L., 2015. Creating concepts from converging features in human cortex. Cerebr. Cortex 25, 2584–2593. https://doi.org/10.1093/cercor/bhu057.

Cui, J., Xu, L., Bressler, S.L., Ding, M., Liang, H., 2008. BSMART: a Matlab/C toolbox for analysis of multichannel neural time series. Neural Network. 21, 1094–1104. https://doi.org/10.1016/j.neunet.2008.05.007.

Cul, A., Baillet, S., Dehaene, S., 2007. Brain dynamics underlying the nonlinear threshold for access to consciousness. PLoS Biol. 5, e260 https://doi.org/10.1371/journal.pbio.0050260.

de Schotten, M., Dell'Acqua, F., Forkel, S.J., Simmons, A., Vergani, F., Murphy, D.G., Catani, M., 2011. A lateralized brain network for visuospatial attention. Nat. Neurosci. 14, 1245. https://doi.org/10.1038/nn.2905.

Dehaene, S., Cohen, L., Morais, J., Kolinsky, R., 2015. Illiterate to literate: behavioural and cerebral changes induced by reading acquisition. Nat. Rev. Neurosci. 16, 234–244. https://doi.org/10.1038/nrn3924.

Dehaene-Lambertz, G., Monzalvo, K., Dehaene, S., 2018. The emergence of the visual word form: longitudinal evolution of category-specific ventral visual areas during reading acquisition. PLoS Biol. 16, e2004103 https://doi.org/10.1371/journal.pbio.2004103.

Delorme, A., Makeig, S., 2004. EEGLAB: an open source toolbox for analysis of single-trial EEG dynamics including independent component analysis. J. Neurosci. Methods 134, 9–21. https://doi.org/10.1016/j.jneumeth.2003.10.009.

Dien, J., 1998. Issues in the application of the average reference: review, critiques, and recommendations. Behav. Res. Methods Instrum. Comput. 30, 34–43. https://doi.org/10.3758/BF03209414.

Eklund, A., Nichols, T.E., Knutsson, H., 2016. Cluster failure: why fMRI inferences for spatial extent have inflated false-positive rates. Proc. Natl. Acad. Sci. 113, 7900–7905. https://doi.org/10.1073/pnas.1602413113.

Fahrenfort, J.J., Lamme, V., 2012. A true science of consciousness explains phenomenology: comment on Cohen and Dennett. Trends Cognit. Sci. 16, 138–139. https://doi.org/10.1016/j.tics.2012.01.004.

Freedman, D.J., Riesenhuber, M., Poggio, T., Miller, E.K., 2003. A comparison of primate prefrontal and inferior temporal cortices during visual categorization. J. Neurosci. 23, 5235–5246. https://doi.org/10.1523/JNEUROSCI.23-12-05235.2003.

Friederici, A.D., 2009. Pathways to language: fiber tracts in the human brain. Trends Cognit. Sci. 13, 175–181. https://doi.org/10.1016/j.tics.2009.01.001.

Garcea, F.E., Chen, Q., Vargas, R., Narayan, D.A., Mahon, B.Z., 2018. Task- and domain-specific modulation of functional connectivity in the ventral and dorsal object-processing pathways. Brain Struct. Funct. 223, 2589–2607. https://doi.org/10.1007/s00429-018-1641-1.

Garcea, F.E., Mahon, B.Z., 2012. What is in a tool concept? Dissociating manipulation knowledge from function knowledge. Mem. Cognit. 40, 1303–1313. https://doi.org/10.3758/s13421-012-0236-y.

Gauthier, I., Curran, T., Curby, K.M., Collins, D., 2003. Perceptual interference supports a non-modular account of face processing. Nat. Neurosci. 6, nn1029. https://doi.org/10.1038/nn1029.

Glezer, L.S., Jiang, X., Riesenhuber, M., 2009. Evidence for highly selective neuronal tuning to whole words in the "visual word form area.". Neuron 62, 199–204. https://doi.org/10.1016/j.neuron.2009.03.017.

Goodale, M.A., 2011. Transforming vision into action. Vis. Res. 51, 1567–1587. https://doi.org/10.1016/j.visres.2010.07.027.

Goodale, M.A., Milner, A.D., 1992. Separate visual pathways for perception and action. Trends Neurosci. 15, 20–25. https://doi.org/10.1016/0166-2236(92)90344-8.

Granger, C., 1969. Investigating causal relations by econometric models and cross-spectral methods. Econometrica 37, 424. https://doi.org/10.2307/1912791.

Grech, R., Cassar, T., Muscat, J., Camilleri, K.P., Fabri, S.G., Zervakis, M., Xanthopoulos, P., Sakkalis, V., Vanrumste, B., 2008. Review on solving the inverse problem in EEG source analysis. J. NeuroEng. Rehabil. 5, 25. https://doi.org/10.1186/1743-0003-5-25.

Gregoriou, G.G., Gotts, S.J., Zhou, H., Desimone, R., 2009. High-frequency, long-range coupling between prefrontal and visual cortex during attention. Science 324, 1207–1210. https://doi.org/10.1126/science.1171402.

Grootswagers, T., Wardle, S.G., Carlson, T.A., 2016. Decoding dynamic brain patterns from evoked responses: a tutorial on multivariate pattern analysis applied to time series neuroimaging data. J. Cognit. Neurosci. 1–21. https://doi.org/10.1162/jocn_a_01068.

Hebart, M.N., Görgen, K., Haynes, J.-D.D., 2014. The Decoding Toolbox (TDT): a versatile software package for multivariate analyses of functional imaging data. Front. Neuroinf. 8, 88. https://doi.org/10.3389/fninf.2014.00088.

Hodges, J.R., Bozeat, S., Ralph, M.A., Patterson, K., Spatt, J., 2000. The role of conceptual knowledge in object use Evidence from semantic dementia. Brain 123, 1913–1925. https://doi.org/10.1093/brain/123.9.1913.

Ishibashi, R., Ralph, M.A., Saito, S., Pobric, G., 2011. Different roles of lateral anterior temporal lobe and inferior parietal lobule in coding function and manipulation tool knowledge: evidence from an rTMS study. Neuropsychologia 49, 1128–1135. https://doi.org/10.1016/j.neuropsychologia.2011.01.004.

Jackson, R.L., Ralph, M.A., Pobric, G., 2015. The timing of anterior temporal lobe involvement in semantic processing. J. Cognit. Neurosci. 27, 1388–1396. https://doi.org/10.1162/jocn_a_00788.

Jefferies, E., 2013. The neural basis of semantic cognition: converging evidence from neuropsychology, neuroimaging and TMS. Cortex 49, 611–625. https://doi.org/10.1016/j.cortex.2012.10.008.

Jiang, X., Bradley, E., Rini, R.A., Zeffiro, T., VanMeter, J., Riesenhuber, M., 2007. Categorization training results in shape- and category-selective human neural plasticity. Neuron 53, 891–903. https://doi.org/10.1016/j.neuron.2007.02.015.

Kravitz, D.J., Saleem, K.S., Baker, C.I., Mishkin, M., 2011. A new neural framework for visuospatial processing. Nat. Rev. Neurosci. 12, 217. https://doi.org/10.1038/nrn3008.

Kravitz, D.J., Saleem, K.S., Baker, C.I., Ungerleider, L.G., Mishkin, M., 2013. The ventral visual pathway: an expanded neural framework for the processing of object quality. Trends Cognit. Sci. 17, 26–49. https://doi.org/10.1016/j.tics.2012.10.011.

Kutas, M., Federmeier, K.D., 2011. Thirty years and counting: finding meaning in the N400 component of the event-related brain potential (ERP). Ann. Rev. Psychol. 62, 621–647. https://doi.org/10.1146/annurev.psych.093008.131123.

Lau, E.F., Phillips, C., Poeppel, D., 2008. A cortical network for semantics: (de) constructing the N400. Nat. Rev. Neurosci. 9, 920–933. https://doi.org/10.1038/nrn2532.

Malone, P.S., Glezer, L.S., Kim, J., Jiang, X., Riesenhuber, M., 2016. Multivariate pattern analysis reveals category-related organization of semantic representations in anterior temporal cortex. J. Neurosci. 36, 10089–10096. https://doi.org/10.1523/JNEUROSCI.1599-16.2016.

Maris, E., Oostenveld, R., 2007. Nonparametric statistical testing of EEG- and MEG-data. J. Neurosci. Methods 164, 177–190. https://doi.org/10.1016/j.jneumeth.2007.03.024.

Maurer, U., Brandeis, D., McCandliss, B.D., 2005. Fast, visual specialization for reading in English revealed by the topography of the N170 ERP response. Behav. Brain Funct. 1, 13. https://doi.org/10.1186/1744-9081-1-13.

Medler, D.A., Binder, J.R., 2005. An on-line orthographic database of the English language. Available from. http://www.neuro.mcw.edu/mcword/. Accessed Sept. 10, 2010.

Mion, M., Patterson, K., Acosta-Cabronero, J., Pengas, G., Izquierdo-Garcia, D., Hong, Y.T., Fryer, T.D., Williams, G.B., Hodges, J.R., Nestor, P.J., 2010. What the left and right anterior fusiform gyri tell us about semantic memory. Brain 133, 3256–3268. https://doi.org/10.1093/brain/awq272.

Nosofsky, R.M., 1986. Attention, similarity, and the identification–categorization relationship. J. Exp. Psychol. Gen. 115, 39. https://doi.org/10.1037/0096-3445.115.1.39.

Papinutto, N., Galantucci, S., Mandelli, M., Gesierich, B., Jovicich, J., Caverzasi, E., Henry, R.G., Seeley, W.W., Miller, B.L., Shapiro, K.A., Gorno -Tempini, M., 2016. Structural connectivity of the human anterior temporal lobe: a diffusion magnetic resonance imaging study. Hum. Brain Mapp. 37, 2210–2222. https://doi.org/10.1002/hbm.23167.

Patterson, K., Nestor, P.J., Rogers, T.T., 2007. Where do you know what you know? The representation of semantic knowledge in the human brain. Nat. Rev. Neurosci. 8, 976–987. https://doi.org/10.1038/nrn2277.

Pegado, F., Comerlato, E., Ventura, F., Jobert, A., Nakamura, K., Buiatti, M., Ventura, P., Dehaene-Lambertz, G., Kolinsky, R., Morais, J., Braga, L.W., Cohen, L., Dehaene, S., 2014. Timing the impact of literacy on visual processing. Proc. Natl. Acad. Sci. U.S.A. 111, E5233–E5242. https://doi.org/10.1073/pnas.1417347111.

Pobric, G., Jefferies, E., Ralph, M.A., 2010. Category-specific versus category-general semantic impairment induced by transcranial magnetic stimulation. Curr. Biol. 20, 964–968. https://doi.org/10.1016/j.cub.2010.03.070.

Pulvermüller, F., 2013. How neurons make meaning: brain mechanisms for embodied and abstract-symbolic semantics. Trends Cognit. Sci. 17, 458–470. https://doi.org/10.1016/j.tics.2013.06.004.

Ralph, M.A., Jefferies, E., Patterson, K., Rogers, T.T., 2016. The neural and computational bases of semantic cognition. Nat. Rev. Neurosci. 18, 42–55. https://doi.org/10.1038/nrn.2016.150.

Riesenhuber, M., Poggio, T., 2002. Neural mechanisms of object recognition. Curr. Opin. Neurobiol. 12, 162–168. https://doi.org/10.1016/S0959-4388(02)00304-5.

Riesenhuber, M., Poggio, T., 2000. Models of object recognition. Nat. Neurosci. 3, 1199–1204. https://doi.org/10.1038/81479.

Rossion, B., Gauthier, I., Goffaux, V., Tarr, M., Crommelinck, M., 2002. Expertise training with novel objects leads to left-lateralized facelike electrophysiological responses. Psychol. Sci. 13, 250–257. https://doi.org/10.1111/1467-9280.00446.

Ruschel, M., Knösche, T.R., Friederici, A.D., Turner, R., Geyer, S., Anwander, A., 2014. Connectivity architecture and subdivision of the human inferior parietal cortex revealed by diffusion MRI. Cerebr. Cortex 24, 2436–2448. https://doi.org/10.1093/cercor/bht098.

Sassenhagen, J., Draschkow, D., 2019. Cluster -based permutation tests of MEG/EEG data do not establish significance of effect latency or location. Psychophysiology e13335. https://doi.org/10.1111/psyp.13335.

Scholl, C.A., Jiang, X., Martin, J.G., Riesenhuber, M., 2013. Time course of shape and category selectivity revealed by EEG rapid adaptation. J. Cognit. Neurosci. 26, 408–421. https://doi.org/10.1162/jocn_a_00477.

Seth, A.K., Barrett, A.B., Barnett, L., 2015. Granger causality analysis in neuroscience and neuroimaging. J. Neurosci. 35, 3293–3297. https://doi.org/10.1523/JNEUROSCI.4399-14.2015.

Tadel, F., Baillet, S., Mosher, J.C., Pantazis, D., Leahy, R.M., 2011. Brainstorm: a user-friendly application for MEG/EEG analysis. Comput. Intell. Neurosci. 2011, 879716. https://doi.org/10.1155/2011/879716.

Tanaka, J., Curran, T., 2001. A neural basis for expert object recognition. Psychol. Sci. 12, 43–47. https://doi.org/10.1111/1467-9280.00308.

Thomas, E., Hulle, M.M., Vogel, R., 2006. Encoding of categories by noncategory-specific neurons in the inferior temporal cortex. J. Cognit. Neurosci. 13, 190–200. https://doi.org/10.1162/089892901564252.

Thorpe, S.J., Fabre-Thorpe, M., 2001. NEUROSCIENCE: seeking categories in the brain. Science 291, 260–263. https://doi.org/10.1126/science.1058249.

Thorpe, S., Fize, D., Marlot, C., 1996. Speed of processing in the human visual system. Am. J. Ophthalmol. 122, 608–609. https://doi.org/10.1016/S0002-9394(14)72148-8.

Vandenberghe, R., Price, C., Wise, R., Josephs, O., Frackowiak, R., 1996. Functional anatomy of a common semantic system for words and pictures. Nature 383, 254–256. https://doi.org/10.1038/383254a0.

Vingerhoets, G., Acke, F., Vandemaele, P., Achten, E., 2009. Tool responsive regions in the posterior parietal cortex: effect of differences in motor goal and target object during imagined transitive movements. Neuroimage 47, 1832–1843. https://doi.org/10.1016/j.neuroimage.2009.05.100.

Wakana, S., Jiang, H., Nagae-Poetscher, L.M., van Zijl, P.C., Mori, S., 2004. Fiber tract–based atlas of human white matter anatomy 1. Radiology 230, 77–87. https://doi.org/10.1148/radiol.2301021640.

Widmann, A., Schröger, E., 2012. Filter effects and filter artifacts in the analysis of electrophysiological data. Front. Psychol. 3, 233. https://doi.org/10.3389/fpsyg.2012.00233.

Woo, C.-W., Krishnan, A., Wager, T.D., 2014. Cluster-extent based thresholding in fMRI analyses: pitfalls and recommendations. Neuroimage 91, 412–419. https://doi.org/10.1016/j.neuroimage.2013.12.058.